















RESEARCH ARTICLE

10.1029/2022JD037883

Different Types of Corona Discharges Associated With High-Altitude Positive Narrow Bipolar Events Nearby Cloud Top

Key Points:

- Corona discharges are found to be associated with unusual high-altitude positive narrow bipolar events nearby cloud top
- Corona discharges are classified into different types according to their different optical and radio features
- The detailed features of corona discharges and their parent thundercloud are estimated using different theoretical models

Dongshuai Li^{1,2} , Alejandro Luque¹ , F. J. Gordillo-Vazquez¹ , F. J. Pérez-Invernón¹ , Lasse Skaaning Husbjerg² , Torsten Neubert² , Olivier Chanrion² , Gaopeng Lu³ , Hongbo Zhang⁴ , Jing Han⁵, Nikolai G. Lehtinen⁶ , Nikolai Østgaard⁶ , and Víctor Reglero⁷ 

¹Instituto de Astrofísica de Andalucía (IAA), CSIC, Granada, Spain, ²National Space Institute, Technical University of Denmark (DTU Space), Kongens Lyngby, Denmark, ³CAS Key Laboratory of Geospace Environment, University of Science and Technology of China, Hefei, China, ⁴Key Laboratory of Middle Atmosphere and Global Environment Observation (LAGEO), Institute of Atmospheric Science, Chinese Academy of Sciences, Beijing, China, ⁵Hainan Institute of Meteorological Sciences, Haikou, China, ⁶Birkeland Centre for Space Science, Department of Physics and Technology, University of Bergen, Bergen, Norway, ⁷Image Processing Laboratory, University of Valencia, Valencia, Spain

Supporting Information:

Supporting Information may be found in the online version of this article.

Correspondence to:

D. Li and A. Luque,
dongshuai@space.dtu.dk;
aluque@iaa.es

Citation:

Li, D., Luque, A., Gordillo-Vazquez, F. J., Pérez-Invernón, F. J., Husbjerg, L. S., Neubert, T., et al. (2023). Different types of corona discharges associated with high-altitude positive narrow bipolar events nearby cloud top. *Journal of Geophysical Research: Atmospheres*, 128, e2022JD037883. <https://doi.org/10.1029/2022JD037883>

Received 21 SEP 2022

Accepted 30 JAN 2023

Abstract Single- and multi-pulse blue corona discharges are frequently observed in thunderstorm clouds. Although we know they often correlate with Narrow Bipolar Events (NBEs) in Very Low Frequency/Low Frequency radio signals, their physics is not well understood. Here, we report a detailed analysis of different types of blue corona discharges observed by the Atmosphere-Space Interactions Monitor during an overpass of a thundercloud cell nearby Malaysia. Both single- and multi-pulse blue corona discharges were associated with positive NBEs at the top of the cloud, reaching about 18 km altitude. We find that the primary pulses of multi-pulse discharges have weaker current moments than the single-pulse discharges, suggesting that the multi-pulse discharges either have shorter vertical channels or have weaker currents than the single-pulse discharges. The subsequent pulse trains of the multi-pulse discharges delayed some milliseconds are likely from horizontally oriented electrical discharges, but some NBEs, correlated with both single- and multi-pulse discharges, include small-amplitude oscillations within a few microseconds inside their waveforms, which are unresolved in the optical observation and yet to be understood. Furthermore, by jointly analyzing the optical and radio observations, we estimate the photon free mean path at the cloud top to be ~6 m.

Plain Language Summary Recent studies indicate that the blue corona discharges detected by the Atmosphere-Space Interactions Monitor onboard the international space station have close association with a special type of intracloud discharges named Narrow Bipolar Events (NBEs). In this study, we present a detailed analysis of different types of NBE-associated corona discharges detected by both optical and radio observations. All the detected corona discharges are found to be associated with unusual high-altitude positive NBEs, which located a few kilometers below the cloud top where the cloud droplets have low impact on the optical observation. This allowed us to infer the physical properties of them and their parent thundercloud by using theoretical models. The results can provide important reference to further investigate the physical mechanism of corona discharge and their role in lightning initiations.

1. Introduction

Blue Luminous Events (BLUEs) are special Transient Luminous Events associated with thunderclouds that radiate intense near-ultraviolet (UV) blue optical emissions dominated by 337 nm with weak or absent signals in the atomic oxygen line at 777.4 nm. They have also been termed as blue corona discharges in the recent studies (Dimitriadou et al., 2022; Husbjerg et al., 2022; Li et al., 2021; F. Liu, Lu, et al., 2021; F. Liu, Zhu, et al., 2021; Soler et al., 2020, 2021, 2022). They have similar features with different phenomena in other studies, such as blue starters/blue jets (Edens, 2011; Kuo et al., 2005; Wescott et al., 1996, 2001), BLEs (Chou et al., 2011, 2018; F. Liu et al., 2018), *glimpses* (Chanrion et al., 2017) and *gnomes* (also called *Pixies*) (Lyons et al., 2003). These optical signals normally last a few to hundreds of milliseconds and appear either isolated or in groups in the active thunderstorms, especially those with overshooting cloud tops and they occurred at the global frequency about 11 s⁻¹ at local midnight (Chanrion et al., 2017; Chou et al., 2018; Dimitriadou et al., 2022; Edens, 2011; Husbjerg et al., 2022; Li, Neubert, et al., 2022; Li et al., 2021; F. Liu, Lu, et al., 2021; F. Liu, Zhu, et al., 2021; Lyons et al., 2003; Soler et al., 2021).

© 2023. The Authors.

This is an open access article under the terms of the [Creative Commons Attribution License](https://creativecommons.org/licenses/by/4.0/), which permits use, distribution and reproduction in any medium, provided the original work is properly cited.

Recently, corona discharges have attracted a lot of attention due to their close correlation with a special type of intracloud (IC) discharges named Compact Intracloud Discharges (CIDs) that emit strong Very High Frequency (VHF) radiation and have the short-duration (tens of microseconds) bipolar-shaped waveforms in the Very Low Frequency/Low Frequency (VLF/LF) band, termed as Narrow Bipolar Events (NBEs) or Narrow Bipolar Pulses (Leal et al., 2019; Le Vine, 1980; Nag & Rakov, 2010a, 2010b; Rison et al., 2016; Smith et al., 1999).

Based on the atmospheric electricity sign convention, NBE can be either positive or negative according to the polarity of first initial half cycle in its electric field waveform (Leal et al., 2019; Willett et al., 1989). The majority of positive NBEs are located at median heights about 13 km between the main negative and upper positive charge regions (Karunarathne et al., 2015; Smith et al., 1999, 2004; Wu et al., 2012, 2014), while the negative NBEs predominantly occur at higher altitudes 14–20 km between the main positive charge region and the screening negative layers (Ahmad et al., 2017; Leal et al., 2019; Smith et al., 1999, 2004; Wu et al., 2012, 2014). However, some negative NBEs are also found to occur at lower altitudes, from 4 to 8 km (Bandara et al., 2019), and a few cases of positive NBEs are also reported to occur at lower altitudes from 5 to 10 km (Wu et al., 2014). Additionally, the altitudes of positive NBEs might be even higher than 16 km, when they are associated with convective surges overshooting the tropopause (Jacobson & Heavner, 2005; Jacobson et al., 2007; Karunarathne et al., 2015; Nag & Rakov, 2010a, 2010b).

NBEs can occur either individually isolated from other lightning discharges within tens of milliseconds (Kostinskiy et al., 2020; Le Vine, 1980; Rison et al., 2016; Smith et al., 1999) or as the lightning initiation event (Karunarathne et al., 2015; López et al., 2022; Lyu et al., 2019; Nag & Rakov, 2010a; Rison et al., 2016; Wu et al., 2011, 2014), or sometime localized in groups (Bandara et al., 2021). The nature of NBEs, and their relation to the formation of the lightning leader is still poorly understood; however, it may provide further insight into the most important problem in lightning physics: the initiation of lightning inside thunderstorms (Rison et al., 2016). Recent observations connected NBEs with a new type of discharge, called fast breakdown (FB), suggesting that NBEs are produced by a system of streamer coronas without a conducting channel or hot leader involved (Lyu et al., 2019; Rison et al., 2016; Tilles et al., 2019), which is further supported by the recent studies of the NBEs-associated BLUEs detected by Atmosphere-Space Interactions Monitor (ASIM) (Li, Luque, Lehtinen, et al., 2022; Li, Neubert, et al., 2022; Li et al., 2021; F. Liu, Lu, et al., 2021; Soler et al., 2020).

In this study, we present a detailed analysis of the different types of corona discharges observed by ASIM during its overpass of an active thundercloud near Malaysia. The BLUEs are found to be associated with unusual high-altitude positive NBEs nearby a deep convective cloud top where the cloud droplets have low impact on the optical observations. This allows us to estimate the detailed features of the corona discharges by jointly analyzing the optical and radio observations.

2. Instruments and Observations

Since 2 April 2018, the Modular Multispectral Imaging Array (MMIA) of the ASIM onboard the International Space Station has provided important insights into Earth thunderstorms from space (Chanrion et al., 2019; Neubert et al., 2019). It includes three photometers with temporal sampling rate at 10^5 samples/s including one in the UV band at 180–230 nm, while the other two are associated with the cameras, in the near-UV at the strongest spectral line of the second positive system of Nitrogen, N_2P (337 nm) and in the strongest lightning emission band, OI (777.4 nm), respectively. The spatial resolution of the cameras on the ground is around 400×400 m with 12 frames per second.

On the evening of 30 April 2020, 21 BLUEs were observed by ASIM when it passed over a thundercloud cell nearby Malaysia during the time period from 17:49:55 UTC to 17:50:55 UTC. All these BLUEs are only detected in the 337 nm photometer and camera, with no or weak signals in the 180–230 nm photometer nor in the 777.4 nm photometer and camera. Among them, 16 BLUEs were captured by both photometers and their corresponding cameras of MMIA, other 5 BLUEs were only captured by the photometers of MMIA without the corresponding camera images. Figure 1 shows the distribution of the cloud-to-ground (CG)/intracloud (IC) lightning and 21 BLUEs (16 with camera images (green square) and 5 without camera images (pink square)) superimposed on the Cloud Top Height (CTH, in km) provided by the Fengyun-4A (FY-4A) satellite (Yang et al., 2017) at the time 17:50:00 UTC (a) and the zoom of its black-dotted rectangular region (b), as well as the 337 nm images detected by MMIA in the zoom region (c). During the time period when the BLUEs occurred, there were a total of 20

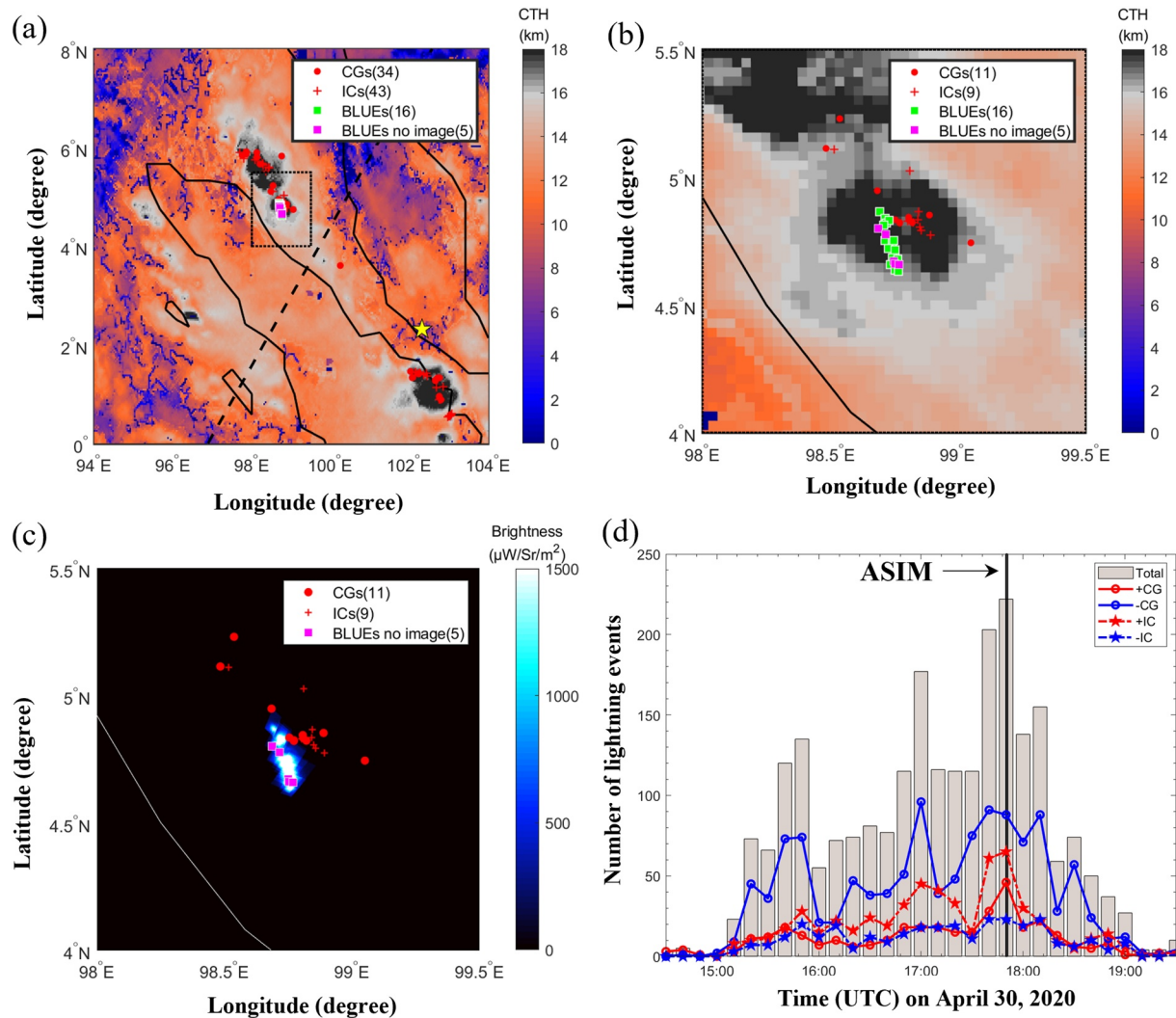


Figure 1. The distribution of 21 BLUEs (16 with camera images (green square) and 5 without camera images (pink square)) along with the cloud-to-ground (red dots)/intracloud (red crosses) lightning on the Cloud Top Height (CTH) at 17:50:00 UTC (a), the zoom of its black-dotted rectangular region (b) and the projected images measured by the 337 nm camera of MMIA in the zoom region (c). In (a), the ground-based Very Low Frequency/Low Frequency sensor at Malaysia is shown as yellow star. The footprints of Atmosphere-Space Interactions Monitor (ASIM) are shown in black dashed line. Numbers of lightning events from 15:00 UTC to 19:00 UTC in the zoom region are shown in (d): positive CGs (+CGs), negative CGs (−CGs), positive ICs (+ICs) and negative ICs (−ICs). The ASIM overpass time is marked in black line.

lightning events with 11 CGs (red dots) and 9 ICs (red crosses) reported by the ground-based Vaisala GLD360 global lightning network (Said & Murphy, 2016) in the zoom region of Figure 1b. The total number of lightning events at the zoom region, shown in Figure 1d, started to increase around 15:00 UTC, then peaked at the time around 17:50 UTC when ASIM passed over. The BLUEs are accompanied by the highest concentration of IC and CG lightnings, which is consistent with previous studies (Chanrion et al., 2017; Husbjerg et al., 2022; Li, Neubert, et al., 2022). The geolocations (latitude and longitude) of the 16 BLUEs are based on the 337 nm images detected by MMIA. For the 5 BLUEs without the corresponding camera images, we use the meta data of 337 nm camera images to find their geolocations. Note that the final geolocations of all the BLUEs have been projected to the cloud top (about 18 km) with a horizontal uncertainty of less than 10 km (Bitzer et al., 2021; Husbjerg et al., 2022; Li, Neubert, et al., 2022).

The broadband VLF/LF magnetic field sensor operates at 400 Hz–400 kHz located at Universiti Teknikal Malaysia Melaka, Malacca, Malaysia (Ahmad et al., 2017; Zhang et al., 2016) (see the yellow star in Figure 1a). After the time of both MMIA and VLF/LF sensor being back-propagated to the BLUE source locations, we evaluate

the time offsets based on the start time between the 337 nm photometer signals and NBE radio pulses. In our case, the time shift for MMIA with respect to the ground-based VLF/LF measurements is within -15 ± 0.6 ms (see Figure S1 in Supporting Information S1).

3. Methodology

3.1. Light-Scattering Model

To simplify the modeling, we assume the corona discharges are impulsive and point-like sources inside a homogeneous isotropic cloud. We fit the 337 nm photometer signal of MMIA based on the first-hitting-time model proposed by Soler et al. (2020) to infer the depth L (relative to the cloud top). The photon flux emitting from the cloud top with the time t_0 being the moment of light emission:

$$f(t) = A \left(\frac{\tau}{t - t_0} \right)^{3/2} \exp(-\tau/(t - t_0) - \nu(t - t_0)), \quad (1)$$

where A is the fitting constant, ν is the collision rate, τ is the characteristic time of diffusion for the depth L between the source and the cloud top. By fitting the 337 nm photometer signal of MMIA, one can obtain the values of the parameters A , t_0 , ν , and τ .

The mean free path Λ with a uniform population of droplets is approximated according to the equations in Thomson and Krider (1982):

$$\Lambda \approx \frac{1}{2\pi r^2 N_d}, \quad (2)$$

where $r = 20 \mu\text{m}$ is the particle radius and $N_d = 1 \times 10^8 \text{ m}^{-3}$ is the particle number density (Luque et al., 2020; Soler et al., 2020).

The depth L can be estimated as:

$$L \approx \sqrt{4\Lambda c \tau / (3(1 - g))} \quad (3)$$

where $g = 0.87$ is the scattering asymmetry parameter and c is the speed of light.

3.2. Electromagnetic Radiation Model

In the simulation, we assume the source of corona discharge as a vertical dipole located at an altitude of H away from observer at a horizontal distance D . The ground is assumed to be perfectly conducting since the corona discharges in our case occurred above the ocean. The magnetic field dB_ϕ for a dipole source is proposed by Uman et al. (1975) and given by:

$$d\vec{B}_\phi(D, t) = \frac{\mu_0 dz'}{4\pi} \sin \theta \left[\frac{i(z', t - R/c)}{R^2} + \frac{1}{cR} \frac{\partial i(z', t - R/c)}{\partial t} \right] \vec{a}_\phi \quad (4)$$

where dz' is the size of the dipole source, c is the speed of light, μ_0 is the magnetic permeability of free space, R is the observation distance between dz' and the observer. θ is the angle between dz' and the vector of the observation distance \vec{R} , $\sin(\theta) = D/R$. \vec{a}_ϕ is the unit vector in ϕ direction. The current $i(t)$ is assumed to be the bi-Gaussian function:

$$i(t) = i_0 \left(e^{-t^2/\tau_1^2} - e^{-t^2/\tau_2^2} \right), \quad (5)$$

where i_0 is the amplitude, τ_1 and τ_2 is the rise time and the fall time, respectively.

The length-integrated current or current moment $M_l(t) = \int i(t) dl$, where l is the length of the lightning current, can be inferred by solving the inverse convolution problem (Cummer, 2003; Cummer & Inan, 2000):

$$B(t) = \int_{-\infty}^{\infty} M_l(\tau) h(t - \tau) d\tau, \quad (6)$$

where $B(t)$ is the measured magnetic field waveform and $h(t)$ is the propagation response evaluated from the modeling results of Equation 4.

4. Results

In this study, we first classify the corona discharges into two groups based on their optical features: single-pulse BLUEs (Li et al., 2021; Soler et al., 2020) and multi-pulse BLUEs (Li, Luque, Lehtinen, et al., 2022; Soler et al., 2020). Both single- and multi-pulse BLUEs are statistically significant with their 337 nm signals above $\mu \pm 5\sigma$ level of the background noise, with absent or negligible signals in both the 180–230 nm photometer and the 777.4 nm photometer (see Appendix A for more details). For the multi-pulse BLUEs, we calculate the binned average of 15 data points (about 150 μ s) of their 337 nm photometer signals (see Appendix B for further details). Figure B1 shows that the secondary optical peaks of all the multi-pulse BLUEs are statistically significant above the standard deviation of preceding signals.

Both single- and multi-pulse BLUEs are associated with positive NBEs (+NBE), then by considering their corresponding radio features, we further classify the BLUEs into four different types, namely (a) single-pulse BLUEs associated with NBEs (BLUE^S), (b) single-pulse BLUEs associated with NBEs including secondary peaks and oscillations (BLUE_{OSC}^S), (c) multi-pulse BLUEs associated with NBEs and their subsequent pulse trains (BLUE^M) and (d) multi-pulse BLUEs associated with oscillated NBEs and their subsequent pulse trains (BLUE_{OSC}^M). For the cases of NBEs with and without oscillations, we estimate the existence of oscillations when the amplitudes of the subsequent radio pulses with the same polarity of the ground wave are above the 3σ level of the background noise (see Appendix C for further details). The small-amplitude oscillations within a few microseconds inside NBE waveforms are marked as “OSC” in the corresponding cases of both single- and multiple-pulse BLUEs in Figures C1 and C2, respectively.

Table 1 shows the detailed feature of the four different types of BLUEs. Among them, there are 10 single-pulse BLUEs and 11 multi-pulse BLUEs, including 4 BLUE^S , 6 BLUE_{OSC}^S , 8 BLUE^M , and 3 BLUE_{OSC}^M . All the BLUEs are found to be isolated from other lightning discharges with no 777.4 nm emission identified by MMIA within at least 100 ms. 5 BLUEs are detected by GLD360 with one identified as +CG and others as +ICs, which are also isolated from other lightning activities. The rise times of the BLUEs change from 0.04 to 0.19 ms with the total time duration ranging from 0.96 to 3.54 ms for the single-pulse BLUEs and to 6.91 ms for the multi-pulse BLUEs. There is no obvious difference for the peak irradiance between the single-pulse and multi-pulse BLUEs.

Further details for all the cases can be found in Figures S2–S22 in Supporting Information S1 with two examples for both single- and multi-pulse BLUEs shown in Figures 2 and 3, respectively. As shown in Figure 2, both BLUE^S and BLUE_{OSC}^S are found to be associated with +NBEs. The waveforms of NBEs in Figures 2c and 2d include the ground wave followed by a 1-hop sky waves, first reflected from the surface of the earth and then from the ionosphere. In our case, since the polarity of the azimuthal magnetic field pointing in the anti-clockwise direction is defined to be positive (Krider et al., 1976; Zhang et al., 2016), based on the atmospheric electricity sign convention, the first initial half cycle of the ground wave of the azimuthal magnetic field is negative for +NBEs.

For the (BLUE^M) in Figure 3, the primary BLUE is found to be associated with a +NBE pulse, but its subsequent optical pulse is found to be associated with several subsequent pulse trains within 3.1 ms. The BLUE_{OSC}^M is found to be similar to (BLUE^M) with NBE pulse and two subsequent optical pulses within 1.4 and 4.4 ms, respectively, but with secondary peaks and microsecond-scale oscillations inside the NBE waveform. The subsequent optical pulses of multi-pulse BLUEs, which followed the primary corona discharges a few milliseconds later, have comparable optical emissions but their associated radio signals are either accompanied by weaker radio emissions or buried in the background noise (see Figures S5, S8, S10, S12, and S19 in Supporting Information S1). Li, Luque, Lehtinen, et al. (2022) discussed the multi-pulse corona discharges related to this study and noted that the subsequent pulse trains of the multi-pulse corona discharges include the electromagnetic pulse pairs that resemble 1-hop sky waves without the ground wave (the red dashed circle outlines the subsequent pulse trains in Figures 3e and 3f), which might emanate from the horizontally oriented corona discharges.

As shown in Table 1, the altitude H of the NBEs are evaluated using the propagation distance and the time delay between the ground wave and 1-hop sky waves in the VLF/LF radio signals based on the simplified ray-theory method (Smith et al., 1999, 2004). The ray path is assumed to follow the rules of geometric optics by propagating in a straight path and being ideally reflected at the ionospheric reflection height in a spherical Earth geometry with an uncertainty about ± 1 km compared to the full-wave method (Li et al., 2020). Previous studies indicate

Table 1

The Detailed Feature of All the BLUEs Occurred at the Time Period From 17:49:55 to 17:50:55 UTC

ID	Flux ($\mu\text{W}/\text{m}^2$)	B_ϕ (nT)	Rise time ^a (ms)	Time duration ^b (ms)	M_i^c (kA · km)	H (km)	Optical L ^d (km)	CTH (km)	Type
27206	2.00	10.84	–	–	24.24	17.23	–	18.46	S with oscillations
27210	6.6	2.19	0.08	2.05	7.48	17.06	1.83	18.60	S
27211	4.54	1.36	0.07	1.56	2.64	17.68	1.61	18.65	M
27213	5.57	2.08	0.12	2.02	5.50	16.67	2.34	18.55	M
27214	10.81	2.75	0.04	0.96	10.08	17.11	1.31	18.55	S with oscillations
27215	13.50	2.58	0.11	2.49	14.89	16.30	2.09	18.67	S with oscillations
27218	5.56	0.69	–	–	1.67	16.69	–	18.60	M
27222	12.42	1.94	0.08	2.73	4.21	17.03	1.82	18.27	M with oscillations
27224	10.28	1.75	–	–	6.23	15.55	–	18.21	M
27225	14.05	3.42	0.19	3.54	7.66	16.65	2.84	18.21	S with oscillations
27231	4.54	1.39	–	–	2.91	15.55	–	17.77	M
27234	6.60	4.49	0.13	2.85	9.18	16.32	2.34	17.50	S
27235	12.96	12.78	0.04	1.01	26.61	17.28	1.34	17.34	S
27236 ^e	8.69	1.38	–	–	3.69	15.87	–	17.47	M
27237	24.77	15.85	0.04	0.99	37.07	17.98	1.27	17.88	S
27238 ^e	10.81	11.15	0.04	0.97	22.62	17.95	1.26	17.04	M
27239	5.56	0.71	0.14	6.91	5.02	16.34	2.42	17.09	M with oscillations
27241	4.54	0.29	0.18	5.69	–	16.54	3.05	17.09	M
27243	3.52	0.60	–	–	–	16.78	–	17.23	S with oscillations
27244	7.12	9.69	0.05	1.26	32.73	17.78	1.48	17.03	S with oscillations
27245	3.01	0.60	–	–	3.59	17.33	–	16.73	M with oscillations

Note. Note that the current moments (M_i) are inferred by solving the inverse convolution problem (Cummer, 2003; Cummer & Inan, 2000) based on the Uman's equation (Uman et al., 1975). The altitudes (H) are estimated using the simplified ray-theory method proposed by Smith et al. (1999, 2004) based on the ground-based VLF/LF sferics. The depths (L) relative to the cloud tops are evaluated by using the first-hitting-time model proposed by Soler et al. (2020) based on the 337 nm photometer signals of MMIA. The Cloud Top Heights (CTHs) are obtained from FY-4A satellite products.

^aRise time is the time taken for the amplitude of a fitted photometer signal to rise from 10% to 90% of the peak. ^bTime duration is the time interval for the amplitude of a fitted photometer signal to rise from 10% and fall to 10% of the peak. ^cThe current moment M_i for ID 27241 and ID 27243 cannot be estimated due to their complex radio signals (see Figures S19 and S20 in Supporting Information S1 for details). ^dFor ID 27224, ID 27231, and ID 27236, there is a small pulse on the rising edge of light-curve that distorted the fit process (see Figures S10, S12, and S15 in Supporting Information S1 for details). The photometer signal is too noisy to be fitted for ID 27206, ID 27243, and ID 27245 (see Figures S2, S20, and S22 in Supporting Information S1 for details). ^eSpecial multi-pulse cases (see Figures S15 and S17 in Supporting Information S1 for details).

that the majority of +NBEs are located at a median height around 13 km, between the main negative and upper positive charge regions (F. Liu, Zhu, et al., 2021; Smith et al., 2004; Wu et al., 2014). However, note that the +NBEs in our study are found to be located at relatively high altitudes, ranging from 15.5 to 18 km near the CTH obtained from the FY-4A satellite (see Table 1).

To further understand the features of the BLUEs, we estimate the depths L (relative to the cloud top) and the current moments M_i based on the light-scattering model and the electromagnetic radiation model in Section 3. In the fitting process, we only fit the BLUEs with clear impulsive pulses and considered as good fitting condition when the coefficient of determination $R^2 > 0.6$ (see green lines in Figures 2a, 2b, and 3a). The modeling light curves agree well with the 337 nm photometer signals of MMIA, indicating the evaluated depths L for the BLUEs are from 1 to 3 km below the cloud top (see Figures S2–S22 in Supporting Information S1). Among them, 3 cases with ID 27206, ID 27243 and ID 27245 are too noisy to be fitted, as well as 3 cases with ID 27224, ID 27231 and ID 27236 contain a small pulse on the rising edge of light-curve that distorted the fitting process (see the footnote in Table 1 for further details).

Figure 4 further shows the correlation between different parameters associated with the BLUEs. Two special cases, whose subsequent pulse trains seem to be “NBE-like” events with ID 27236 and ID 27238, are marked by

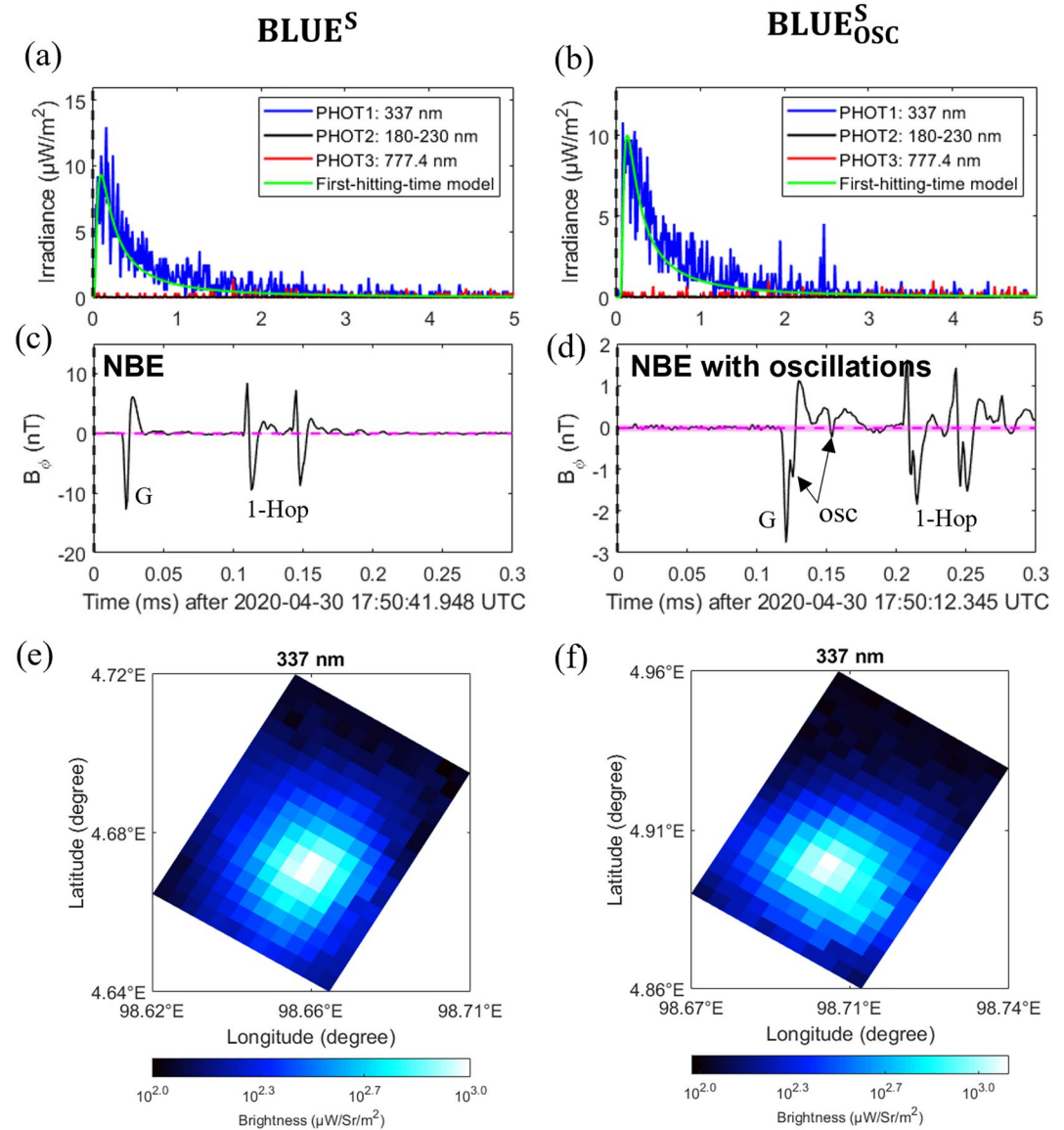


Figure 2. Examples of the single-pulse BLUEs associated with NBEs (BLUE^S) for ID 27235 (a, c, e) and the single-pulse BLUEs associated with NBEs including secondary peaks and oscillations (BLUE^S_{osc}) for ID 27214 (b, d, f). MMIA photometer irradiance (blue: 337 nm, black: 180–230 nm, red: 777.4 nm and green: modeling result of the first-hitting-time model) (a, b) and its corresponding radio signal detected from the ground-based Very Low Frequency/Low Frequency sensor nearby Malaysia (c, d). The 337 nm images of MMIA are shown in the (e) and (f). The pink horizontal dashed line is the mean of the background noises with the pink shaded band $\mu \pm 3\sigma$ in (c), (d). The oscillations are marked as OSC in (d). The ground wave and the ionospheric 1-hop sky waves are marked as G and 1-Hop in (c), (d), respectively.

green dots. They might be two NBE events that occurred closely in time (see Figures S15 and S17 in Supporting Information S1), however, it is too noisy to identify them through the radio signals.

As shown in Figure 4a, the rise times of MMIA photometer signals have an obvious correlation with the altitudes H of NBEs. This might be due to the high-altitude + NBEs in our study are located only a few kilometers below the cloud top where the cloud droplets have relatively low impact on the MMIA measurements. Figure 4b shows a linear correlation between the radio-signal inferred altitude H and the parameter $\eta = \sqrt{4c\tau/(3(1-g))}$ evaluated from the MMIA photometer signals. According to Equation 3, the photon mean free path at the cloud top can be obtained by using $\Lambda = 1/(0.4)^2 \approx 6$ m, where $0.4 \text{ m}^{1/2}$ is the slope of the fitting line in Figure 4b. This is consistent with the photon mean free path $\Lambda \approx 4$ m assumed in the previous studies by considering the particle radius $r = 20 \text{ }\mu\text{m}$ and the number density $N_d = 1 \times 10^8 \text{ m}^{-3}$ (Li et al., 2021; Luque et al., 2020; Soler et al., 2020).

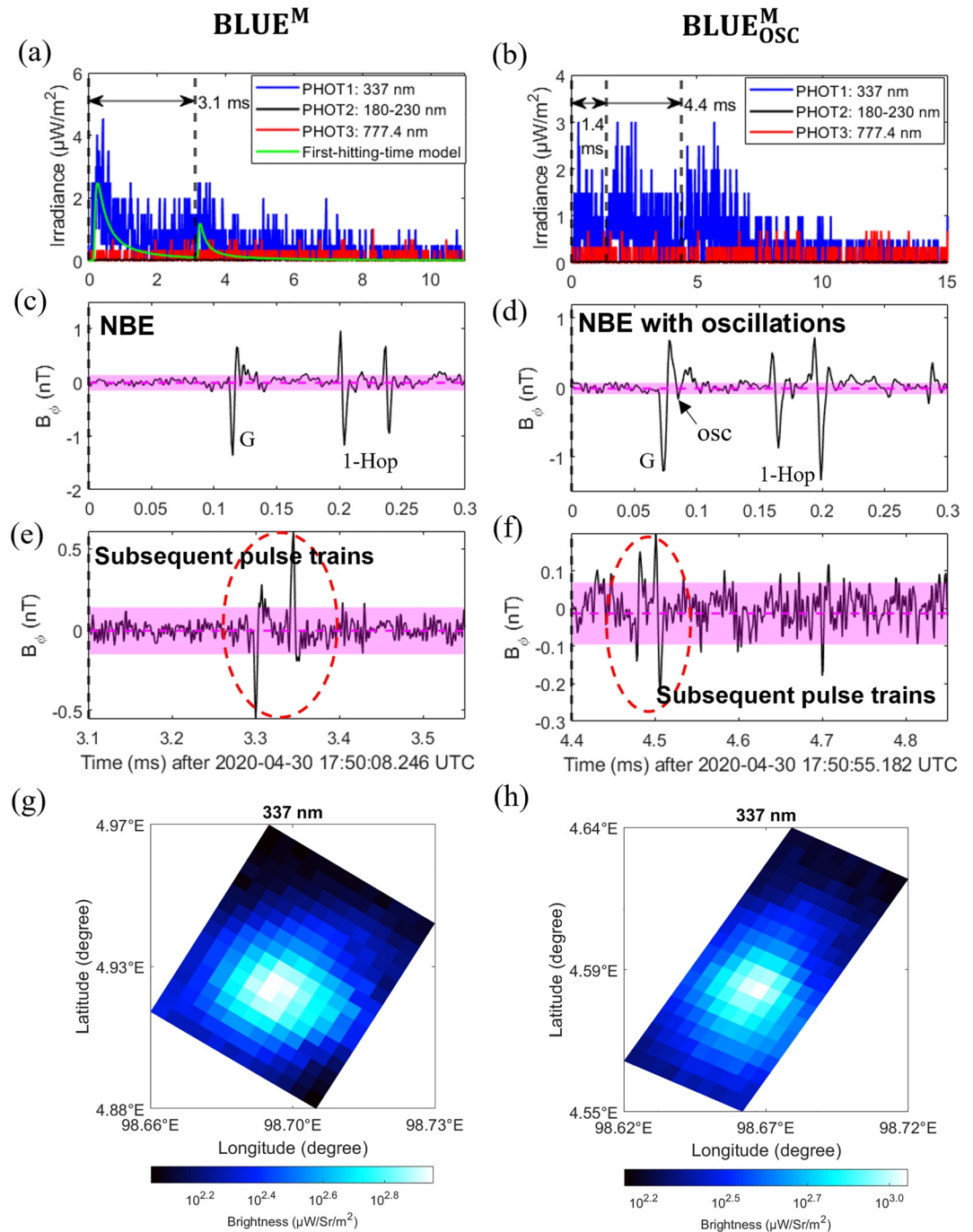


Figure 3. Similar to Figure 2, but for the multi-pulse BLUEs associated with NBEs and their subsequent pulse trains (marked in the red dashed circle region) ($BLUE^M$) for ID 27211 (a, c, e, g) and the multi-pulse BLUEs associated with oscillated NBEs and their subsequent pulse trains (marked in the red dashed circle region) ($BLUE^M_{osc}$) for ID 27245 (b, d, f, h). Note that (f) only shows the subsequent pulse trains after 4.4 ms since the radio signals after 1.4 ms are not obvious and might overlap with the multiple-hop ionospheric reflections of NBEs (see Figure S22 in Supporting Information S1). The pink horizontal dashed line is the mean of the background noises with the pink shaded band $\mu \pm 3\sigma$ in (c, d, e, f). The oscillations are marked as OSC in (d). The ground wave and the ionospheric 1-hop sky waves are marked as G and 1-Hop in (c), (d), respectively.

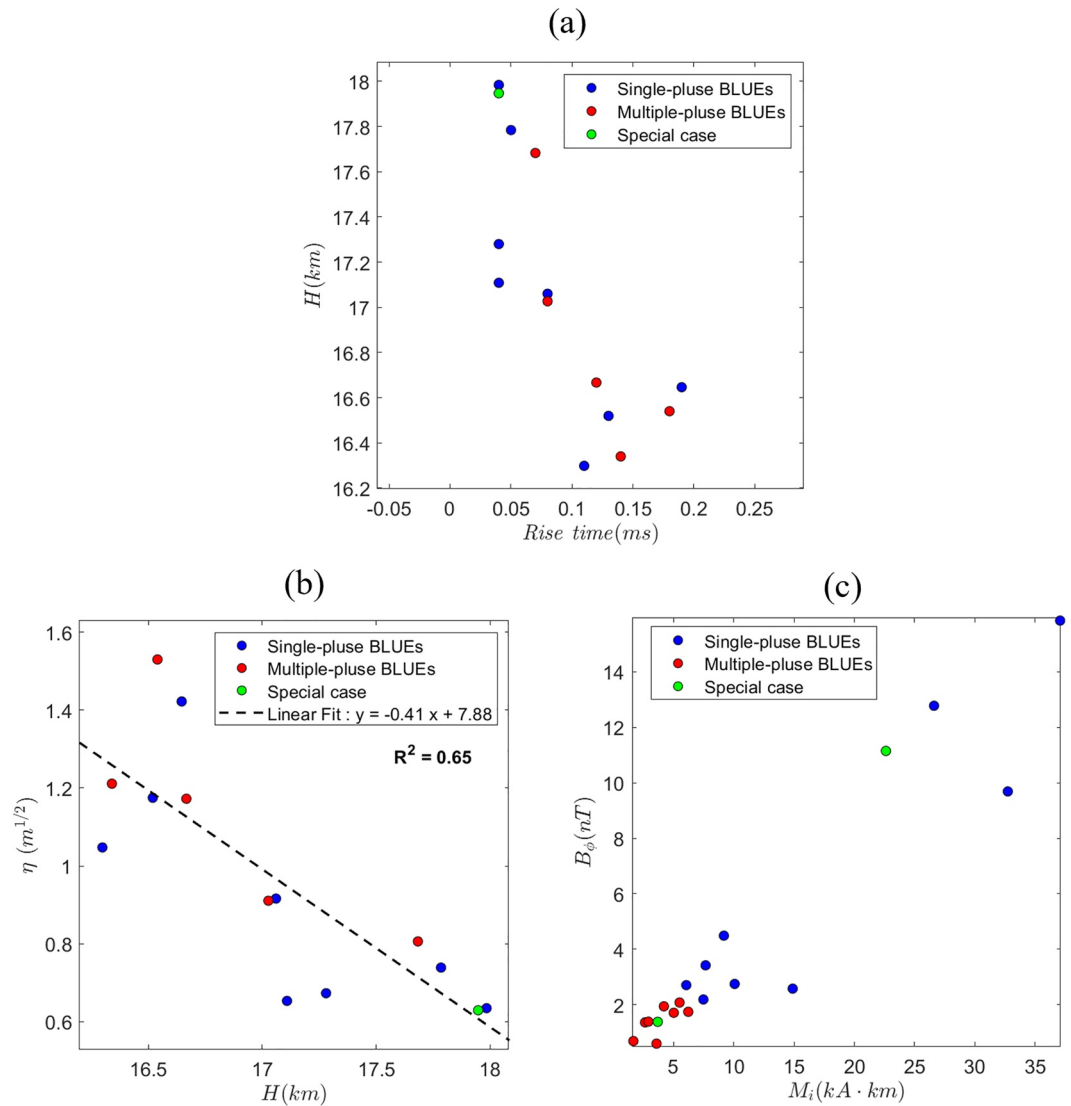


Figure 4. The correlation of (a) the rise time of 337 nm photometer signal and the altitude of NBEs (H), (b) the altitude of NBEs (H) and the parameter $\eta = \sqrt{4c\tau/(3(1-g))}$ and (c) the current moment (M_i) and the magnetic field strength (B_ϕ). The single- and multi-pulse BLUEs are shown in blue and red dots, respectively. The 2 special multi-pulse cases for ID 27236 and ID 27238 are marked as green dots.

Moreover, as expected, the amplitude of the azimuthal magnetic field component B_ϕ and the estimated current moment M_i show a tight linear relationship in Figure 4c. Despite one special case, the current moments and the magnetic fields of the NBEs corresponding to the multi-pulse BLUEs (red dots) are found to be weaker than those related to the single-pulse BLUEs (blue dots). It suggests that the multi-pulse BLUEs either have shorter vertical channels or have weaker currents than the single-pulse BLUEs.

5. Discussion and Summary

In this study, we first classify 21 BLUEs near the cloud top of a localized thunderstorm into two groups based on their optical features: Single-pulse BLUEs (10) and multi-pulse BLUEs (11). Then by considering their corresponding radio features, we further classify them into four different types including (a) the single-pulse BLUEs associated with NBEs ($BLUE^S$), (b) the single-pulse BLUEs associated with NBEs including secondary peaks and oscillations ($BLUE^S_{OSC}$), (c) the multi-pulse BLUEs associated with NBEs and their subsequent pulse trains ($BLUE^M$) and (d) the multi-pulse BLUEs associated with oscillated NBEs and their subsequent pulse trains ($BLUE^M_{OSC}$).

Both single- and multi-pulse BLUEs are found to be associated with unusual high-altitude + NBEs nearby the cloud top. Both the CTH image (see Figure 1) and the ring structures in the 337 nm camera image indicated that there is an overshooting convective cloud top associated with the corona discharges (see Figures S10 and S11 in Supporting Information S1). In our case, the high-altitude + NBEs might occur between the positive charge lifted to relatively high altitude by the strong updraft and the negative screening charge layer near the overshooting cloud top (Li, Luque, Lehtinen, et al., 2022; MacGorman et al., 2017).

The subsequent pulse trains of the multi-pulse BLUEs, which followed the NBEs a few milliseconds later, are either accompanied by weaker radio emissions or buried in the background noise. As discussed in Li, Luque, Lehtinen, et al. (2022), they might emanate from the horizontally oriented corona discharges. The results indicate that the NBEs associated with the multi-pulse BLUEs might have similar features with the initiation-type NBEs (INBEs) (Wu et al., 2014), but interestingly, all the NBEs in our study are so-called isolated NBEs which does not trigger full-edged lightning.

Some NBEs, correlated with both single- and multi-pulse BLUEs, included microsecond-scale oscillations inside their waveforms. Recent studies indicate that the fast breakdowns of NBEs sometimes contain secondary fast breakdowns along the previous path (Attanasio et al., 2021; Li, Luque, Gordillo-Vázquez et al., 2022; Rison et al., 2016; Tilles et al., 2019). Most recent observations from the LOw Frequency ARray (LOFAR) also indicate that multiple, spatially distributed corona bursts can occur in lightning processes with a timescale of 10 μ s (N. Liu et al., 2022). The feature of secondary peaks and the microsecond-scale oscillations might be a fundamental property in NBE radio waveforms (Hamlin et al., 2007; Karunarathne et al., 2015; Leal & Rakov, 2019; Nag & Rakov, 2009). However, the optical signals in our case are affected by scattering effect and the 10 μ s temporal sampling rate of MMIA which is not high enough to show this feature. Therefore, it is yet to be understood.

Previous studies indicate that both positive and negative streamers could be involved in the fast breakdowns of CIDs emitting NBEs and overlap within a significant volume (Huang et al., 2021; Li, Luque, Gordillo-Vázquez et al., 2022; Lyu et al., 2019; Rison et al., 2016; Tilles et al., 2019). The microsecond-scale oscillations of NBEs are observed in both single- and multi-pulse BLUEs, which suggests that the BLUEs might be produced by the fast breakdowns consisting of both positive and negative streamers. It is unclear whether the polarity of the streamers contributes to the differences in different types of BLUEs in our study.

The current moments of the multi-pulse BLUEs are found to be weaker than those related to the single-pulse BLUEs. Since the current moments are evaluated by assuming the sources to be vertical dipoles, it suggests that the multi-pulse BLUEs either have shorter vertical channels or have weaker currents than the single-pulse BLUEs. However, the results of our study are based on a localized thundercloud cell nearby Malaysia, additional studies are required in order to determine whether the features are general or particular.

The estimated altitudes of the +NBEs range from 15.5 to 18 km, near the cloud top where the cloud droplets have relatively low impact on the MMIA measurements. Nevertheless, by fitting the correlation between the radio-signal inferred altitude H and the parameter $\eta = \sqrt{4c\tau/(3(1-g))}$ evaluated from the optical signals, we estimate the photon mean free path at the cloud top $\Lambda \approx 6$ m, which is consistent with the findings of a recent study (Li, Neubert, et al., 2022). In their study, Li, Neubert, et al. (2022) showed that most of the corona discharges are located close to high ice water content with a photon mean free path $\Lambda \approx 3$ m measured by the Cloud-Aerosol Lidar and Infrared Pathfinder Satellite Observation. However, note that both particle radius and the number density can be strongly affected by the deep convection inside the thunderstorm (Brunner & Bitzer, 2020; Li, Neubert, et al., 2022). To further investigate the cloud microphysics and its effect on the corona discharges, a more detailed light-scattering model including a parameterization of cloud microphysics is required in future studies.

Appendix A: The Statistical Significance of Photometer Signals Detected by MMIA

In this appendix, we estimate the statistical significance of the three photometer signals detected by MMIA. The mean μ and standard deviation σ for the background signal are calculated by using 1,000 data points (10 ms) before the first primary BLUE begins. In our case, both single-pulse and multi-pulse BLUEs are statistically significant with their 337 nm signals above $\mu \pm 5\sigma$ level of the background noise, with absent or negligible

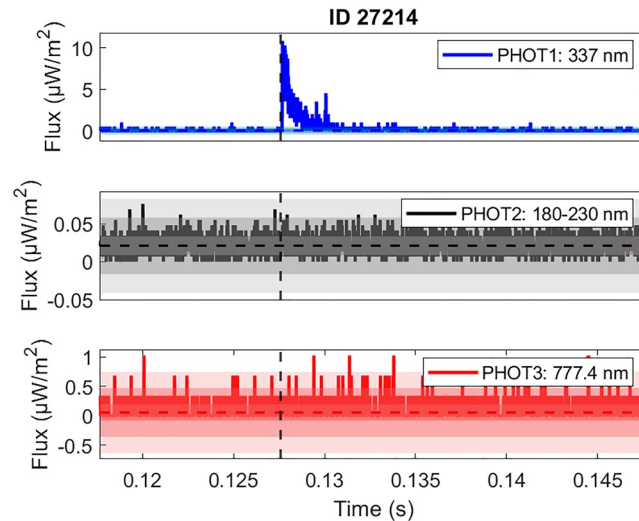


Figure A1. The statistical significance of the photometer signals of a single-pulse BLUE with ID 27214 (corresponding to Figure 2a) (Blue: 337 nm, Black: 180–230 nm, and Red: 777.4 nm). The black vertical dashed line marked the start time for the BLUE pulse. The horizontal dashed line is the mean of the background noises with the shaded bands indicating $\mu \pm \sigma$, $\mu \pm 3\sigma$, and $\mu \pm 5\sigma$.

signals in both the 180–230 nm photometer and the 777.4 nm photometer. Figures A1 and A2 give examples of the statistical significance of the photometer signals of a single-pulse BLUE with ID 27214 (corresponding to Figure 2a) and a multi-pulse BLUE with ID 27211 (corresponding to Figure 3a), respectively.

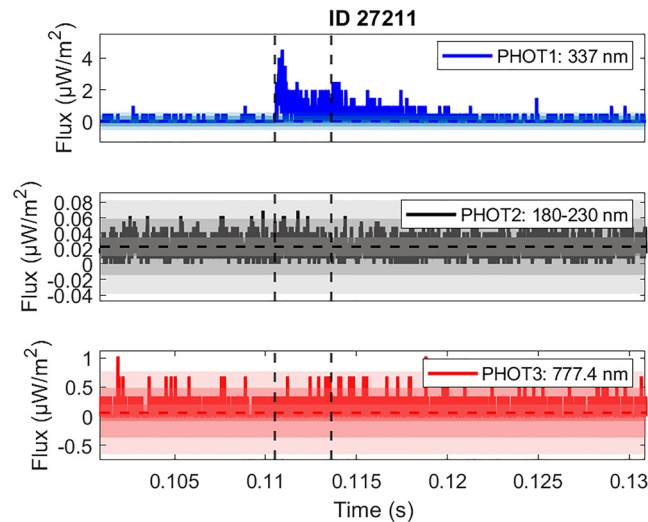


Figure A2. Similar to Figure A1, but for a multi-pulse BLUE case with ID 27211 (corresponding to Figure 3a). The black vertical dashed lines marked the start time for the primary and secondary BLUE pulses.

Appendix B: The Statistical Significance of Multi-Pulse Corona Discharges

In this appendix, we calculate the binned average of 15 data points (corresponding to 150 μ s) of the 337 nm photometer signal to estimate the statistical significance of all the multi-pulse BLUEs. For each bin we compute the standard deviation of the samples within the bin and plot the estimated standard deviation of the mean (standard deviation of the samples inside the bin divided by the square root of the number of samples). In most

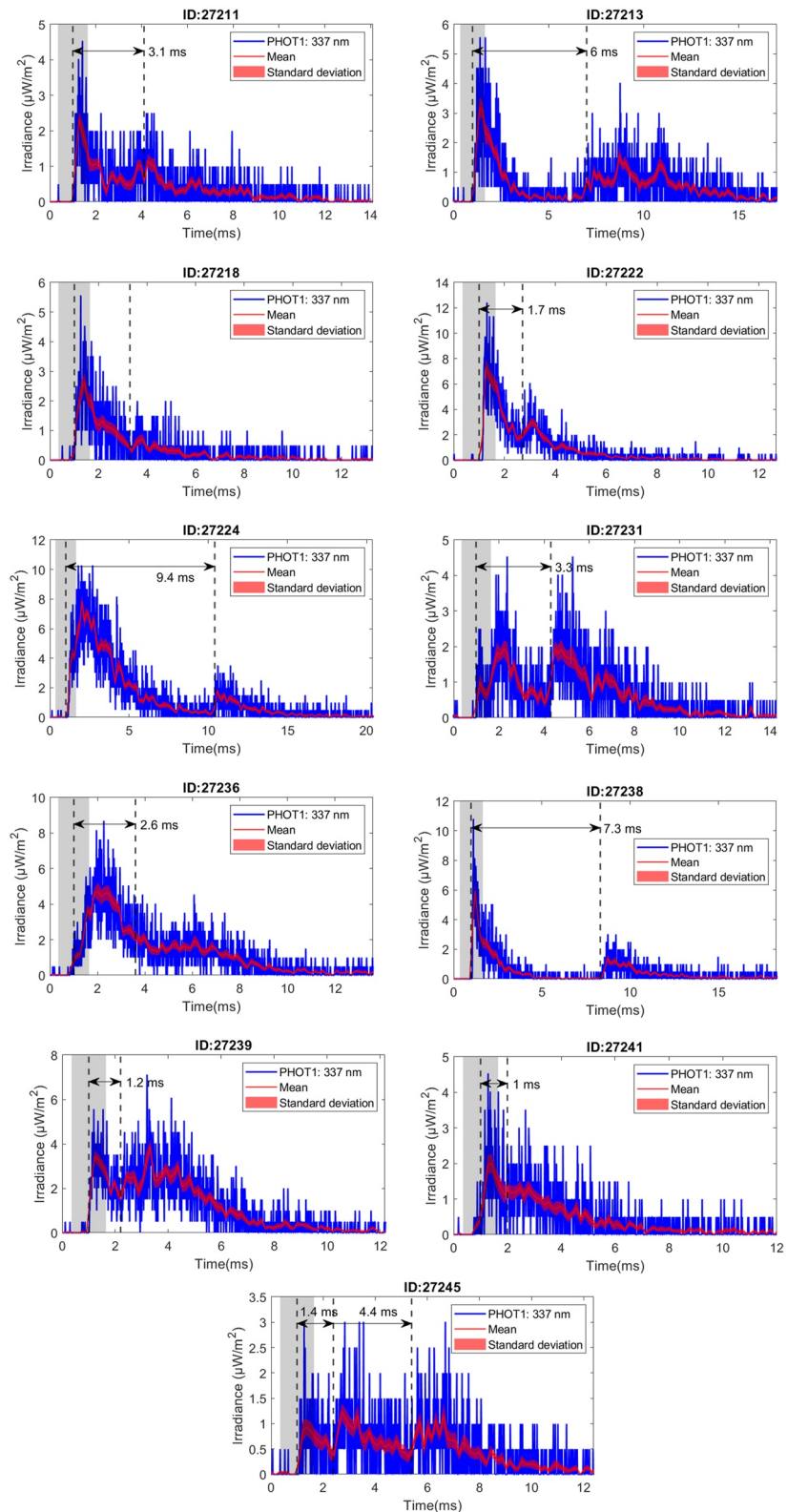


Figure B1. The binned average of 15 data points (corresponding to 150 μs) of the 337 nm photometer signals for multi-pulse BLUEs. The mean and standard deviation of the sample mean are marked in the red solid line and its shaded band. The start time (refer to source) for NBE and its subsequent pulse is marked in dashed black line with ± 0.65 ms uncertainty (gray shadowed region).

of cases, the secondary peaks of multi-pulse BLUEs are statistically significant. The event with ID 27236, where the two pulses overlap but are identifiable nevertheless, is corresponding to one special case where the subsequent pulse trains look very much like a negative NBE, however, it is too noisy to identify it through the radio signals (see Figure S15 in Supporting Information S1).

See Figure B1

Appendix C: The Statistical Significance of the Oscillation Features in Radio Signals

In this appendix, we analyze the statistical significance of the NBE radio pulses for both single- and multi-pulse BLUEs. The mean μ and standard deviation σ for the background signal are calculated by using radio signals within 10 ms before the NBE event begins. We estimate the existence of oscillations when the amplitudes of the subsequent radio pulses in the same polarity of the ground wave are outside $\mu - 3\sigma$ level of the background noise. The NBE radio signals with and without oscillation features for single- and multi-pulse BLUEs are shown in Figures C1 and C2 respectively.

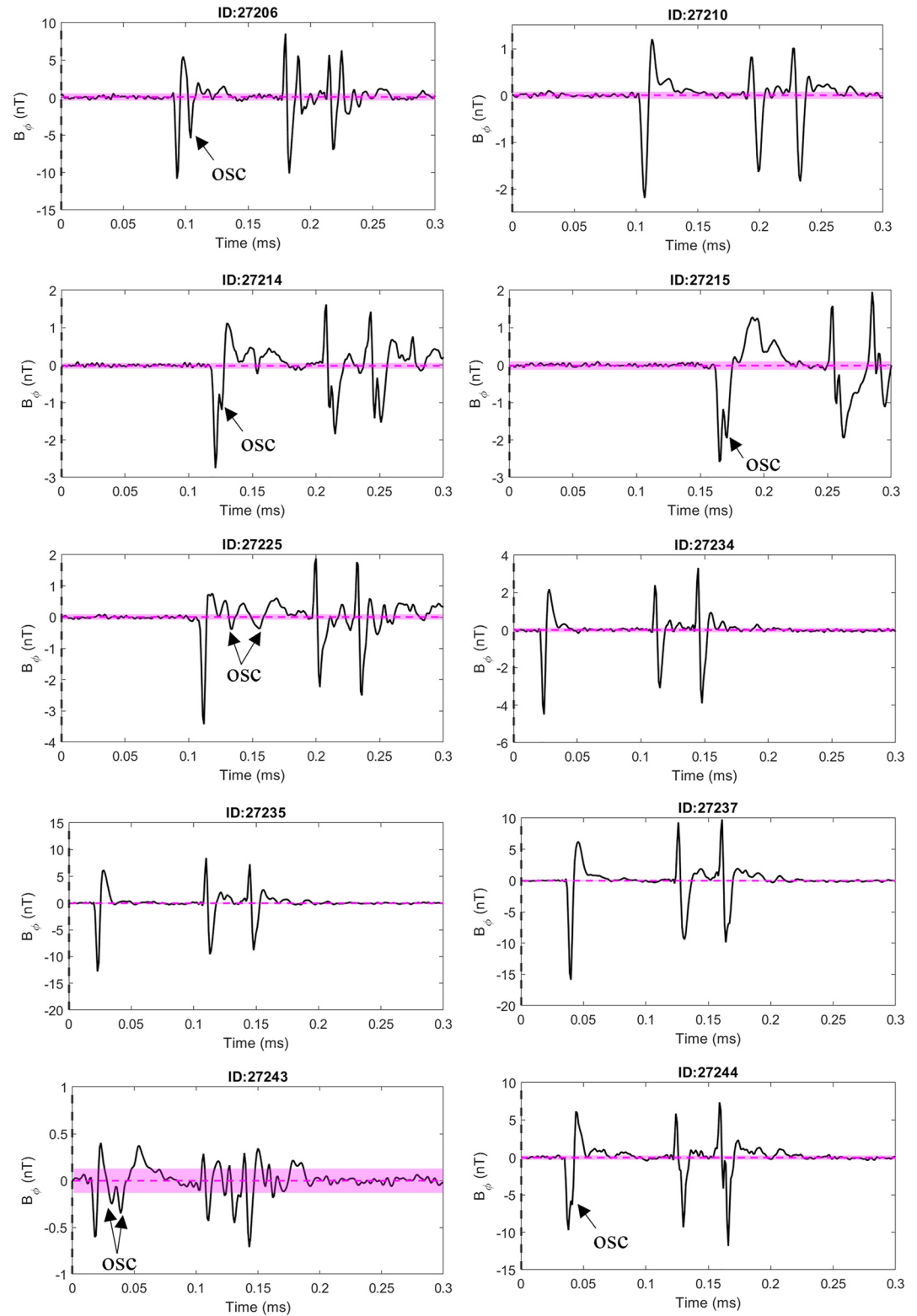


Figure C1. The statistical significance of the oscillation of the NBE radio pulses for all the single-pulse BLUEs. The pink horizontal dashed line is the mean of the background noises with the pink shaded band $\mu \pm 3\sigma$. The oscillations are marked as OSC in the corresponding cases.

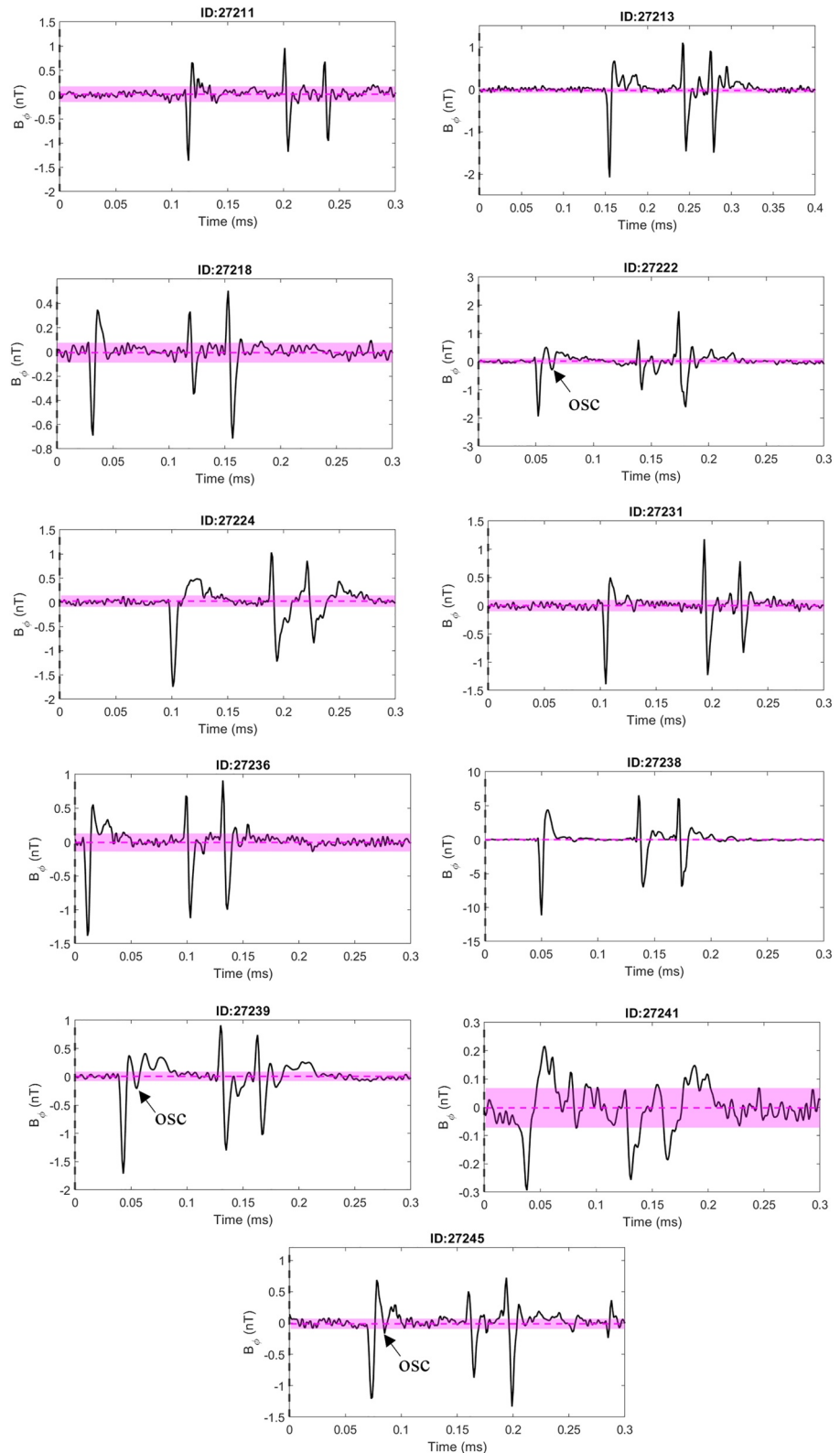


Figure C2. Similar to C1, but for the NBE radio pulses of all the multi-pulse BLUEs. The horizontal dashed line is the mean of the background noises with the pink shaded band $\mu \pm 3\sigma$. The oscillations are marked as OSC in the corresponding cases.

Data Availability Statement

The Modular Multispectral Imaging Array (MMIA) level 1 data and Global Lightning Detection Network GLD360 data were obtained from <https://asdc.space.dtu.dk/>. ASIM data is proprietary and not currently available for public release. Interested parties should direct their data request to the ASIM Science Data Centre (asdc@space.dtu.dk). The Fengyun-4A (FY-4A) satellite data is public to the registered user by contacting (dataserver@cma.gov.cn) and supplied by the FENGYUN satellite Data Center (<http://satellite.nsmc.org.cn/PortalSite/Data/Satellite.aspx?currentculture=en-US>). The VLF/LF radio data that support the findings of this study are openly available at (<https://doi.org/10.5281/zenodo.7096902>).

Acknowledgments

This work was supported by the European Research Council (ERC) under the European Union H2020 programme/ERC Grant agreement 681257. It also received funding from the European Union Horizon 2020 research and innovation programme under the Marie Skłodowska-Curie Grant agreement SAINT 722337. Additionally, this work was supported by the Spanish Ministry of Science and Innovation, MINECO, under project PID2019-109269RB-C43 and FEDER program. D.L. would like to acknowledge the Independent Research Fund Denmark (Danmarks Frie Forskningsfond) under Grant agreement 1026-00420B. D.L., A.L., F.J.G.V. and F.J.P.I. would like to acknowledge financial support from the State Agency for Research of the Spanish MCIU through the “Center of Excellence Severo Ochoa” award for the Instituto de Astrofísica de Andalucía (SEV-2017-0709). G.L. is supported by the Chinese Meridian Project, and the International Partnership Program of Chinese Academy of Sciences (No.183311KYSB20200003). ASIM is a mission of the European Space Agency (ESA) and is funded by ESA and by national grants of Denmark, Norway and Spain. The ASIM Science Data Centre is supported by ESA PRODEX contracts C 4000115884 (DTU) and 4000123438 (Bergen).

References

- Ahmad, M. R., Periannan, D., Sabri, M. H. M., Aziz, M. Z. A. A., Lu, G., Zhang, H., et al. (2017). Emission heights of narrow bipolar events in a tropical storm over the Malacca Strait. In *2017 international conference on electrical engineering and computer science (ICECOS)* (pp. 305–309). <https://doi.org/10.1109/ICECOS.2017.8167155>
- Attanasio, A., da Silva, C., & Krehbiel, P. (2021). Electrostatic conditions that produce fast breakdown in thunderstorms. *Journal of Geophysical Research: Atmospheres*, *126*(19), e2021JD034829. <https://doi.org/10.1029/2021JD034829>
- Bandara, S., Marshall, T., Karunarathne, S., Karunarathne, N., Siedlecki, R., & Stolzenburg, M. (2019). Characterizing three types of negative narrow bipolar events in thunderstorms. *Atmospheric Research*, *219*, 105450. <https://doi.org/10.1016/j.atmosres.2019.05.013>
- Bandara, S., Marshall, T., Karunarathne, S., & Stolzenburg, M. (2021). Groups of narrow bipolar events within thunderstorms. *Atmospheric Research*, *252*, 105450. <https://doi.org/10.1016/j.atmosres.2021.105450>
- Bitzer, P. M., Walker, T. D., Lang, T. J., Gatlin, P. N., Chanrion, O., Neubert, T., et al. (2021). Multifrequency optical observations of lightning with ISS-LIS and ASIM. In *Agu fall meeting 2021*.
- Brunner, K. N., & Bitzer, P. M. (2020). A first look at cloud inhomogeneity and its effect on lightning optical emission. *Geophysical Research Letters*, *47*(10), e2020GL087094. <https://doi.org/10.1029/2020GL087094>
- Chanrion, O., Neubert, T., Mogensen, A., Yair, Y., Stendel, M., Singh, R., & Siingh, D. (2017). Profuse activity of blue electrical discharges at the tops of thunderstorms. *Geophysical Research Letters*, *44*(1), 496–503. <https://doi.org/10.1002/2016GL071311>
- Chanrion, O., Neubert, T., Rasmussen, I. L., Stoltz, C., Tcherniak, D., Jessen, N. C., et al. (2019). The Modular Multispectral Imaging Array (MMIA) of the ASIM payload on the international space station. *Space Science Reviews*, *215*(4), 1–25. <https://doi.org/10.1007/s11214-019-0593-y>
- Chou, J. K., Hsu, R.-R., Su, H.-T., Chen, A. B.-C., Kuo, C.-L., Huang, S.-M., et al. (2018). ISUAL-observed blue luminous events: The associated sferics. *Journal of Geophysical Research: Space Physics*, *123*(4), 3063–3077. <https://doi.org/10.1002/2017JA024793>
- Chou, J. K., Tsai, L. Y., Kuo, C. L., Lee, Y. J., Chen, C. M., Chen, A. B., et al. (2011). Optical emissions and behaviors of the blue starters, blue jets, and gigantic jets observed in the Taiwan transient luminous event ground campaign. *Journal of Geophysical Research*, *116*(A7), A07301. <https://doi.org/10.1029/2010ja016162>
- Cummer, S. A. (2003). Current moment in sprite-producing lightning. *Journal of Atmospheric and Solar-Terrestrial Physics*, *65*(5), 499–508. (Sprites, Elves and their Global Activities). [https://doi.org/10.1016/S1364-6826\(02\)00318-8](https://doi.org/10.1016/S1364-6826(02)00318-8)
- Cummer, S. A., & Inan, U. S. (2000). Modeling ELF radio atmospheric propagation and extracting lightning currents from ELF observations. *Radio Science*, *35*(2), 385–394. <https://doi.org/10.1029/1999RS002184>
- Dimitriadou, K., Chanrion, O., Neubert, T., Protat, A., Louf, V., Heumesser, M., et al. (2022). Analysis of blue corona discharges at the top of tropical thunderstorm clouds in different phases of convection. *Geophysical Research Letters*, *49*(6), e2021GL095879. <https://doi.org/10.1029/2021GL095879>
- Edens, H. E. (2011). Photographic and lightning mapping observations of a blue starter over a New Mexico thunderstorm. *Geophysical Research Letters*, *38*(17), L17804. <https://doi.org/10.1029/2011GL048543>
- Hamlin, T., Light, T. E., Shao, X. M., Eack, K. B., & Harlin, J. D. (2007). Estimating lightning channel characteristics of positive narrow bipolar events using intrachannel current reflection signatures. *Journal of Geophysical Research*, *112*(D14), D14108. <https://doi.org/10.1029/2007JD008471>
- Huang, A., Cummer, S. A., & Pu, Y. (2021). Lightning initiation from fast negative breakdown is led by positive polarity dominated streamers. *Geophysical Research Letters*, *48*(8), e2020GL091553. <https://doi.org/10.1029/2020GL091553>
- Husbjerg, L. S., Neubert, T., Chanrion, O., Dimitriadou, K., Li, D., Stendel, M., et al. (2022). Observations of blue corona discharges in thunderclouds. *Geophysical Research Letters*, *49*(12), e2022GL099064. <https://doi.org/10.1029/2022GL099064>
- Jacobson, A. R., Boeck, W., & Jeffery, C. (2007). Comparison of narrow bipolar events with ordinary lightning as proxies for the microwave-radiometry ice-scattering signature. *Monthly Weather Review*, *135*(4), 1354–1363. <https://doi.org/10.1175/mwr3342.1>
- Jacobson, A. R., & Heavner, M. J. (2005). Comparison of narrow bipolar events with ordinary lightning as proxies for severe convection. *Monthly Weather Review*, *133*(5), 1144–1154. <https://doi.org/10.1175/MWR2915.1>
- Karunarathne, S., Marshall, T. C., Stolzenburg, M., & Karunarathna, N. (2015). Observations of positive narrow bipolar pulses. *Journal of Geophysical Research: Atmospheres*, *120*(14), 7128–7143. <https://doi.org/10.1002/2015JD023150>
- Kostinskiy, A. Y., Marshall, T. C., & Stolzenburg, M. (2020). The mechanism of the origin and development of lightning from initiating event to initial breakdown pulses (v.2). *Journal of Geophysical Research: Atmospheres*, *125*(22), e2020JD033191. <https://doi.org/10.1029/2020JD033191>
- Krider, E. P., Noggle, R. C., & Uman, M. A. (1976). A gated, wideband magnetic direction finder for lightning return strokes. *Journal of Applied Meteorology and Climatology*, *15*(3), 301–306. [https://doi.org/10.1175/1520-0450\(1976\)015<301:agwmdf>2.0.co;2](https://doi.org/10.1175/1520-0450(1976)015<301:agwmdf>2.0.co;2)
- Kuo, C.-L., Hsu, R. R., Chen, A. B., Su, H. T., Lee, L. C., Mende, S. B., et al. (2005). Electric fields and electron energies inferred from the ISUAL recorded sprites. *Geophysical Research Letters*, *32*(19), L19103. <https://doi.org/10.1029/2005GL023389>
- Leal, A. F., & Rakov, V. A. (2019). A study of the context in which compact intracloud discharges occur. *Scientific Reports*, *9*(1), 1–15. <https://doi.org/10.1038/s41598-019-48680-6>
- Leal, A. F., Rakov, V. A., & Rocha, B. R. (2019). Compact intracloud discharges: New classification of field waveforms and identification by lightning locating systems. *Electric Power Systems Research*, *173*, 251–262. <https://doi.org/10.1016/j.eprsr.2019.04.016>
- Le Vine, D. M. (1980). Sources of the strongest RF radiation from lightning. *Journal of Geophysical Research*, *85*(C7), 4091–4095. <https://doi.org/10.1029/JC085iC07p04091>

- Li, D., Liu, F., Pérez-Invernón, F. J., Lu, G., Qin, Z., Zhu, B., & Luque, A. (2020). On the accuracy of ray-theory methods to determine the altitudes of intracloud electric discharges and ionospheric reflections: Application to narrow bipolar events. *Journal of Geophysical Research: Atmospheres*, *125*(9), e2019JD032099. <https://doi.org/10.1029/2019JD032099>
- Li, D., Luque, A., Gordillo-Vázquez, F. J., Liu, F., Lu, G., Neubert, T., et al. (2021). Blue flashes as counterparts to narrow bipolar events: The optical signal of shallow in-cloud discharges. *Journal of Geophysical Research: Atmospheres*, *126*(13), e2021JD035013. <https://doi.org/10.1029/2021JD035013>
- Li, D., Luque, A., Gordillo-Vázquez, F. J., Silva, C. D., Krehbiel, P. R., Rachidi, F., & Rubinstein, M. (2022). Secondary fast breakdown in narrow bipolar events. *Geophysical Research Letters*, *49*(7), e2021GL097452. <https://doi.org/10.1029/2021GL097452>
- Li, D., Luque, A., Lehtinen, N. G., Gordillo-Vázquez, F. J., Neubert, T., Lu, G., et al. (2022). Multi-pulse corona discharges in thunderclouds observed in optical and radio bands. *Geophysical Research Letters*, *49*(13), e2022GL098938. <https://doi.org/10.1029/2022GL098938>
- Li, D., Neubert, T., Husbjerg, L., Zhu, Y., Chanrion, O., Lapierre, J., et al. (2022). Observation of corona discharges and cloud microphysics at the top of thunderstorm cells in cyclone Fani. *Earth and Space Science Open Archive*, *15*. <https://doi.org/10.1002/essoar.10512239.1>
- Liu, F., Lu, G., Neubert, T., Lei, J., Chanrion, O., Østgaard, N., et al. (2021). Optical emissions associated with narrow bipolar events from thunderstorm clouds penetrating into the stratosphere. *Nature Communications*, *12*(6631), 6631. <https://doi.org/10.1038/s41467-021-26914-4>
- Liu, F., Zhu, B., Lu, G., Lei, J., Shao, J., Chen, Y., et al. (2021). Meteorological and electrical conditions of two mid-latitude thunderstorms producing blue discharges. *Journal of Geophysical Research: Atmospheres*, *126*(8), e2020JD033648. <https://doi.org/10.1029/2020JD033648>
- Liu, F., Zhu, B., Lu, G., Qin, Z., Lei, J., Peng, K.-M., et al. (2018). Observations of blue discharges associated with negative narrow bipolar events in active deep convection. *Geophysical Research Letters*, *45*(6), 2842–2851. <https://doi.org/10.1002/2017GL076207>
- Liu, N., Scholten, O., Dwyer, J. R., Hare, B. M., Sterpka, C. F., Tilles, J. N., & Lind, F. D. (2022). Implications of multiple corona bursts in lightning processes for radio frequency interferometer observations. *Geophysical Research Letters*, *49*(7), e2021GL097367. <https://doi.org/10.1029/2021GL097367>
- López, J. A., Montanyà, J., van der Velde, O., Romero, D., Gordillo-Vázquez, F. J., Pérez-Invernón, F. J., et al. (2022). Initiation of lightning flashes simultaneously observed from space and the ground: Narrow bipolar events. *Atmospheric Research*, *268*, 105981. <https://doi.org/10.1016/j.atmosres.2021.105981>
- Luque, A., Gordillo-Vázquez, F. J., Li, D., Malagón-Romero, A., Pérez-Invernón, F. J., Schmalzried, A., et al. (2020). Modeling lightning observations from space-based platforms (CloudScat.jl 1.0). *Geoscientific Model Development*, *13*(11), 5549–5566. <https://doi.org/10.5194/gmd-13-5549-2020>
- Lyons, W. A., Nelson, T. E., Armstrong, R. A., Pasko, V. P., & Stanley, M. A. (2003). Upward electrical discharges from thunderstorm tops. *Bulletin of the American Meteorological Society*, *84*(4), 445–454. <https://doi.org/10.1175/bams-84-4-445>
- Lyu, F., Cummer, S. A., Qin, Z., & Chen, M. (2019). Lightning initiation processes imaged with very high frequency broadband interferometry. *Journal of Geophysical Research: Atmospheres*, *124*(6), 2994–3004. <https://doi.org/10.1029/2018JD029817>
- MacGorman, D. R., Elliott, M. S., & DiGangi, E. (2017). Electrical discharges in the overshooting tops of thunderstorms. *Journal of Geophysical Research: Atmospheres*, *122*(5), 2929–2957. <https://doi.org/10.1002/2016JD025933>
- Nag, A., & Rakov, V. A. (2009). Electromagnetic pulses produced by bouncing-wave-type lightning discharges. *IEEE Transactions on Electromagnetic Compatibility*, *51*(3), 466–470. <https://doi.org/10.1109/TEMC.2009.2025495>
- Nag, A., & Rakov, V. A. (2010a). Compact intracloud lightning discharges: 1. Mechanism of electromagnetic radiation and modeling. *Journal of Geophysical Research*, *115*(D20), D20102. <https://doi.org/10.1029/2010JD014235>
- Nag, A., & Rakov, V. A. (2010b). Compact intracloud lightning discharges: 2. Estimation of electrical parameters. *Journal of Geophysical Research*, *115*(D20), D20103. <https://doi.org/10.1029/2010JD014237>
- Neubert, T., Østgaard, N., Reglero, V., Blanc, E., Chanrion, O., Oxborrow, C. A., et al. (2019). The ASIM mission on the international space station. *Space Science Reviews*, *215*(2), 1–17. <https://doi.org/10.1007/s11214-019-0592-z>
- Rison, W., Krehbiel, P. R., Stock, M. G., Edens, H. E., Shao, X.-M., Thomas, R. J., et al. (2016). Observations of narrow bipolar events reveal how lightning is initiated in thunderstorms. *Nature Communications*, *7*(1), 10721. [https://doi.org/10.1038/ncomms10721\(2016\)](https://doi.org/10.1038/ncomms10721(2016))
- Said, R., & Murphy, M. (2016). GLD360 upgrade: Performance analysis and applications. In *24th international lightning detection conference*.
- Smith, D. A., Heavner, M. J., Jacobson, A. R., Shao, X. M., Massey, R. S., Sheldon, R. J., & Wiens, K. C. (2004). A method for determining intracloud lightning and ionospheric heights from VLF/LF electric field records. *Radio Science*, *39*(1), RS1010. <https://doi.org/10.1029/2002RS002790>
- Smith, D. A., Shao, X. M., Holden, D. N., Rhodes, C. T., Brook, M., Krehbiel, P. R., et al. (1999). A distinct class of isolated intracloud lightning discharges and their associated radio emissions. *Journal of Geophysical Research*, *104*(D4), 4189–4212. <https://doi.org/10.1029/1998JD200045>
- Soler, S., Gordillo-Vázquez, F. J., Pérez-Invernón, F. J., Luque, A., Li, D., Neubert, T., et al. (2021). Global frequency and geographical distribution of nighttime streamer corona discharges (BLUEs) in thunderclouds. *Geophysical Research Letters*, *48*(18), e2021GL094657. <https://doi.org/10.1029/2021GL094657>
- Soler, S., Gordillo-Vázquez, F. J., Pérez-Invernón, F. J., Luque, A., Li, D., Neubert, T., et al. (2022). Global distribution of key features of streamer corona discharges in thunderclouds. *Journal of Geophysical Research: Atmospheres*, *127*, e2022JD037535. <https://doi.org/10.1029/2022JD037535>
- Soler, S., Pérez-Invernón, F. J., Gordillo-Vázquez, F. J., Luque, A., Li, D., Malagón-Romero, A., et al. (2020). Blue optical observations of narrow bipolar events by ASIM suggest corona streamer activity in thunderstorms. *Journal of Geophysical Research: Atmospheres*, *125*(16), e2020JD032708. <https://doi.org/10.1029/2020JD032708>
- Thomson, L. W., & Krider, E. P. (1982). The effects of clouds on the light produced by lightning. *Journal of the Atmospheric Sciences*, *39*(9), 2051–2065. [https://doi.org/10.1175/1520-0469\(1982\)039<textless{ }2051:TEOCOT-textgreater{ }2.0.CO;2](https://doi.org/10.1175/1520-0469(1982)039<textless{ }2051:TEOCOT-textgreater{ }2.0.CO;2)
- Tilles, J. N., Liu, N., Stanley, M. A., Krehbiel, P. R., Rison, W., Stock, M. G., et al. (2019). Fast negative breakdown in thunderstorms. *Nature Communications*, *10*(1), 1–12. <https://doi.org/10.1038/s41467-019-09621-z>
- Uman, M. A., McLain, D. K., & Krider, E. P. (1975). The electromagnetic radiation from a finite antenna. *American Journal of Physics*, *43*(1), 33–38. <https://doi.org/10.1119/1.10027>
- Wescott, E. M., Sentman, D. D., Heavner, M. J., Hampton, D. L., Osborne, D. L., & Vaughan, O. H., Jr. (1996). Blue starters Brief upward discharges from an intense Arkansas thunderstorm. *Geophysical Research Letters*, *23*(16), 2153–2156. <https://doi.org/10.1029/96GL01969>
- Wescott, E. M., Sentman, D. D., Stenbaek-Nielsen, H. C., Huet, P., Heavner, M. J., & Moudry, D. R. (2001). New evidence for the brightness and ionization of blue starters and blue jets. *Journal of Geophysical Research*, *106*(A10), 21549–21554. <https://doi.org/10.1029/2000JA000429>
- Willett, J. C., Bailey, J. C., & Krider, E. P. (1989). A class of unusual lightning electric field waveforms with very strong high-frequency radiation. *Journal of Geophysical Research*, *94*(D13), 16255–16267. <https://doi.org/10.1029/JD094iD13p16255>
- Wu, T., Dong, W., Zhang, Y., Funaki, T., Yoshida, S., Morimoto, T., et al. (2012). Discharge height of lightning narrow bipolar events. *Journal of Geophysical Research*, *117*(D5). <https://doi.org/10.1029/2011JD017054>

- Wu, T., Dong, W., Zhang, Y., & Wang, T. (2011). Comparison of positive and negative compact intracloud discharges. *Journal of Geophysical Research*, 116(D3), D03111. <https://doi.org/10.1029/2010JD015233>
- Wu, T., Yoshida, S., Ushio, T., Kawasaki, Z., & Wang, D. (2014). Lightning-initiator type of narrow bipolar events and their subsequent pulse trains. *Journal of Geophysical Research: Atmospheres*, 119(12), 7425–7438. <https://doi.org/10.1002/2014JD021842>
- Yang, J., Zhang, Z., Wei, C., Lu, F., & Guo, Q. (2017). Introducing the new generation of Chinese geostationary weather satellites, Fengyun-4. *Bulletin of the American Meteorological Society*, 98(8), 1637–1658. <https://doi.org/10.1175/bams-d-16-0065.1>
- Zhang, H., Lu, G., Qie, X., Jiang, R., Fan, Y., Tian, Y., et al. (2016). Locating narrow bipolar events with single-station measurement of low-frequency magnetic fields. *Journal of Atmospheric and Solar-Terrestrial Physics*, 143–144, 88–101. <https://doi.org/10.1016/j.jastp.2016.03.009>